

In Situ Reconfigurable Continuum Robot with Varying Curvature Enabled by Programmable Tensegrity Building Blocks

Jie Zhang, Junhao Shi, Junhai Huang, Qihuan Wu, Yuwen Zhao, Jinzhao Yang, Hamed Rajabi, Zhigang Wu,* Haijun Peng,* and Jianing Wu*

Reconfigurable continuum robots exhibit programmable interaction capability, enabling them to cope with challenges poorly addressed by conventional rigid robots. However, the regulation of the module type and/or sequence may result in time-consuming and labor-intensive problems. Therefore, in situ reconfiguration schemes are required to develop in a simple yet robust solution for continuum robot design. Herein, inspired by the structure characteristics of the seahorse tail, an original template based on a tensegrity building block (TBB) for creating an in situ reconfigurable continuum robotic paradigm is proposed. As the length of the stretchable struts in the TBB could be programmed, five typical homologous types from the template are derived. Then, ten TBBs into a continuum robot are assembled and the multi-body dynamic framework is employed to develop a mechanical model for predicting the profile after deformation. Theoretical predictions demonstrate that the robotic shape can be customized in situ by switching the type of TBBs, without disassembling the robot. Furthermore, the tailored continuum robotic configurations are applied to conformally interact with the varying-curvature objects. The experimental results suggest that the proposed programmable template offers a facile and rapid reconfiguration scheme for the continuum robots, which greatly improves the robotic interaction capability.

These continuum robots extend the interaction capabilities of conventional rigid robots because of their inherent compliance, demonstrating great promise in many applications, such as minimally invasive surgeries,^[2] research operations,^[3] and detection in unstructured environments.^[4] The existing continuum robots can be classified into three typical categories in terms of actuation, namely, the pneumatic-driven,^[5] smart material-driven,^[6] and cable-driven robots.^[7]

Pneumatic-driven continuum robots, which are powered by compressed gas or fluid, cannot be used to make compact and lightweight robotic systems. Smart material-driven robots have also limited output force that impedes their usability in human environments.^[8] In contrast, the cable-driven continuum robots have attracted the interests of engineers because of their both high payload and fairly high kinematic accuracy, enabling the cable-driven robots to become one of the most used one in application.^[9]

To balance the high structural compliance and strong carrying capacity of the cable-driven robots, these continuum robots are required to be fabricated by combining materials with varying mechanical properties.^[10] Therefore, a classical continuum robotic configuration was proposed by Buckingham, which consisted of an elastic backbone equipped with rigid constraint disks equidistant.^[11] Owing to the

1. Introduction

Inspired by biological appendages, such as elephant trunks and octopus tentacles, the concept of continuum robots, first proposed by Robinson, represents a class of robotic configurations that possess theoretically infinite degrees of freedom (DOFs).^[1]

J. Zhang, J. Shi, J. Huang, Q. Wu, Y. Zhao, J. Yang, Z. Wu, J. Wu
School of Aeronautics and Astronautics
Shenzhen Campus of Sun Yat-Sen University
Shenzhen 518107, P. R. China
E-mail: wuzhigang@mail.sysu.edu.cn; wujn27@mail.sysu.edu.cn

H. Rajabi
Division of Mechanical Engineering and Design
School of Engineering
London South Bank University
London SE1 0AA, UK

 The ORCID identification number(s) for the author(s) of this article can be found under <https://doi.org/10.1002/aisy.202300048>.

H. Peng
School of Mechanical Engineering
Dalian University of Technology
Dalian 116024, P. R. China
E-mail: hjpeng@dlut.edu.cn

© 2023 The Authors. Advanced Intelligent Systems published by Wiley-VCH GmbH. This is an open access article under the terms of the Creative Commons Attribution License, which permits use, distribution and reproduction in any medium, provided the original work is properly cited.

J. Wu
School of Advanced Manufacturing
Shenzhen Campus of Sun Yat-Sen University
Shenzhen 518107, P. R. China

DOI: 10.1002/aisy.202300048

utilization of elastic materials, this robot is able to exhibit a compliant circle-shaped profile while actuating cables.^[12] However, as these cable-driven continuum robots always demonstrate relatively homogeneous deformation behaviors, the invariant robotic curvature may result in mismatching during the interaction, hindering the highly efficient interaction in varying scenarios.^[13]

To enhance the interaction efficiency in unstructured environments, programming the robotic curvature has become a promising solution for continuum robots.^[14] These tailored configurations are generally constructed by combining graduated material properties and/or structures.^[15] For example, Zhang et al. developed a bio-inspired continuum robot by integrating springs with varying stiffness into a modular tensegrity structure.^[16] As the structural stiffness significantly varies between the modules, the robotic curvature can be programmed to conformally interact with varying environments. In addition, Ke et al. presented a programmable robotic paradigm that was constructed by discretely presetting graded structural properties to enhance the interaction efficiency.^[13] However, these configurations are of great difficulty to be changed ad tuned once generated.^[17] Hence, each continuum robot has its unique shape and can perform specific tasks only.^[18] Introducing a simple reconstruction strategy into continuum robotic design can help to overcome this challenge.^[19]

Reconfigurable robotic profile enables continuum robots to adjust their physical properties depending on the requirements of each application.^[20] For example, Santoso et al. proposed a modular continuum robot that is capable of both deployable extension and bending deformation achieved through an origami-inspired design.^[21] This continuum robot can be scaled up by optionally adding robotic modules on-demand because each module can be controlled independently, without modification to the system architecture, demonstrating a more robust interaction capability to adapt to varying scenarios. However, the embedded actuators installed in each module would result in uneven mass distribution, which may reduce the control accuracy.^[22] Therefore, continuum robots are often equipped with a remotely centralized actuation system.^[23] An example of this was underactuated modular continuum robot developed by Bishop et al.^[24] As the configuration is constructed by an identical module, the robot can merely reconfigure a limited number of profiles, which may hinder the continuum robot to interact with complex and changeable scenarios. To overcome this limitation, Atia et al. proposed a design method to create diverse building blocks for enriching the robotic module type.^[6] Therefore, the robotic configuration can be preprogrammed on-demand by assembling varying building blocks. These building blocks can also be disassembled and reconfigured to facilitate the reconfigurability from one assembled robot to another. However, this reconfigurable route may result in time-consuming and labor-intensive problems during regulating the type/sequence of the modules.

Herein, inspired by the structural characteristics of the seahorse tail, we proposed an original template for constructing an in situ reconfigurable continuum robot based on a tensegrity building block (TBB) which consists of transverse, longitudinal, and stretchable struts (**Figure 1**). The components of the TBB are fabricated by 3D printing, which not only simplifies the robotic production but also reduces the costs, facilitating future

community uptakes. By programming the length of the stretchable struts, we derived five typical homologous types from the TBB template. To elaborate on the effects of this programmable TBB for enhancing the interaction capability of the continuum robot, we first assembled ten TBBs into a continuum robot and formulated a mechanical model using multi-body dynamic framework to predict the profiles after deformation. Theoretical predictions demonstrate that our continuum robotic profile can be programmed in situ by switching the types of the TBBs, without disassembling the continuum robot. Then, we utilized the tailored continuum robotic configurations to interact with the varying-curvature objects conformally. The experimental results suggest that our proposed programmable TBB offers a facile and rapid reconstruction paradigm for the development of continuum robots, which can improve the robotic interaction capability.

2. Results and Discussion

2.1. Structural Characteristics of Seahorse Tail

A seahorse is featured by its unique morphology and special swimming style, enabling it to become one of the most remarkable sea creatures (**Figure 2A**).^[25] We focused on the seahorse tail because this agile appendage enables the slow-moving seahorse to survive in complex marine environments. The tail is composed of several subdermal bony plates arranged in articulated ring-like segments.^[26] By measuring the dimension of the segments, we assumed that these structurally analogous segments might be derived from an identical structural template by programming the geometrical parameters (**Figure S1**, Supporting Information). As the dimension of the segments declines from the base to the tip of the tails, these homologous segments have different inertia moments I_y . Assuming the same elasticity modulus E for all the segments, the equivalent bending stiffness $K_B = EI_y$ of the basal segment is ≈ 130.96 times that of the distal one; therefore, the distal end of the tapered tail can curl more easily during grasping (**Figure 2B**, **Video S1**, Supporting Information).^[27] This result indicates that programming the dimensions of a defined building block, independent of the material properties, results in varying mechanical properties. This understanding can inspire a paradigm for the development of programmable building blocks for in situ reconfigurable continuum robots.

2.2. Bio-Inspired TBB

Inspired by the structural characteristics of the seahorse tail, we proposed a cuboid TBB as a programmable template, as shown in **Figure 1**. The template with the physical dimensions of length l , width w , and height h contains two square ring-like layers, which are alternately connected by two transverse and two stretchable struts. Four longitudinal struts are divided into two groups to link to the adjacent layers by rotary hinges. In the template, each stretchable strut is composed of an inner rod, an outer rod, and two modulation buttons. As the outer rod is equipped with five assembly positions, the length of the stretchable strut can be modulated as 40, 45, 50, 55, and 60 mm. Hence, the TBB exhibits five typical homologous types by programming the length of the

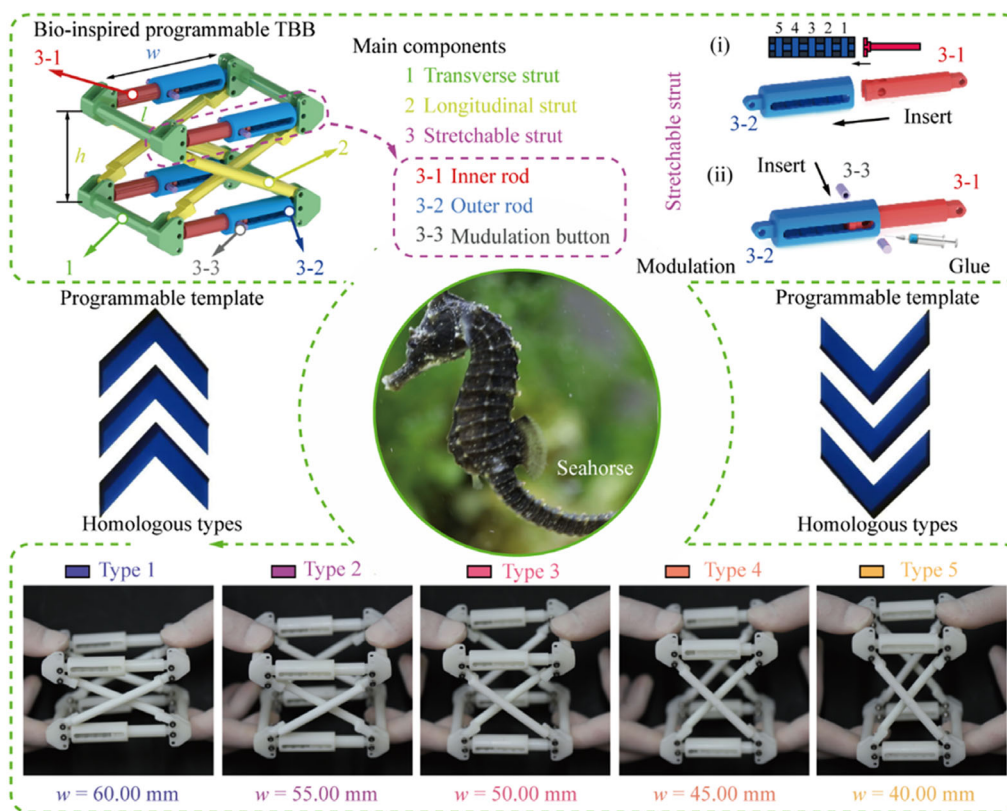


Figure 1. Bio-inspired programmable TBB. Programmable TBB composing of transverse, longitudinal, and stretchable struts. Each stretchable strut contains an inner rod, an outer rod, and two modulation buttons. Five typical homologous types derived from the TBB.

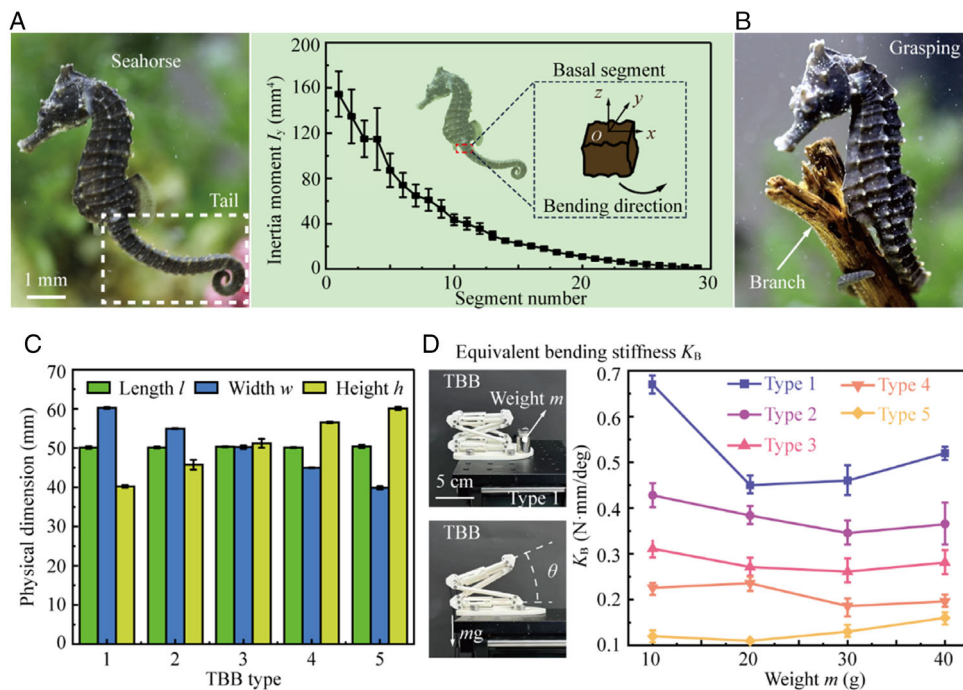


Figure 2. Physical characteristics of the bio-inspired TBB. A) Inertia moment of each segment in a seahorse tail. B) Seahorse tail configuring a bending profile for grasping a branch. C) Physical dimensions of the homologous types. D) Equivalent bending stiffness of the homologous types.

stretchable strut, namely, types 1–5 (Figure S2, Supporting Information).^[28] To distinguish these TBBs easily, we also employed five single-color blocks to describe the typical homologous types, as shown in Figure 1.

Then, we fabricated these types by 3D printing and measured the corresponding physical dimensions $l-w-h$ of each type, as shown in Figure 2C (Table S1, Supporting Information). Then, we quantified the equivalent bending stiffness K_B of the types and found that the structural stiffness declined with the decrease in the length of the stretchable struts (Figure 2D). Here, the diverse types of TBB exhibit different trends of stiffness variation with increasing weight, which may be caused by both the strong structural geometric nonlinearity and the difference in the friction force. By comparing the experimental results, the stiffness of the type 1 reaches $0.52 \pm 0.09 \text{ N mm degree}^{-1}$, which is about 3.98 times that of type 5. This result indicates that the mechanical property of our bio-inspired TBB can be programmed by regulating the dimension. Therefore, when continuum robots were constructed by the template, we could regulate the local mechanical property on demand by switching the type of the TBB and accomplish in situ reconstruction for continuum robots.

2.3. Continuum Robot with In Situ Reconfigurable Characteristics

We first developed a continuum robotic prototype by assembling ten TBBs, in all of which the initial configurations were set to be type 1, and then used four tension cables (No. 1–4) that passed through the corresponding preexisting holes of each TBB to actuate the robot (Con. 1), as shown in Figure 3A. When the length variation of the cables satisfies the actuation criterion of $\Delta l_s : \Delta l_r = 5 : 1$, our continuum robot is able to bend about the Y-axis in the XOZ plane, transforming into a specific curved profile from the initially straight shape (Figure 3B, Video S2,

Supporting Information). Here, we extracted the robotic distal end trajectories from both experimental and predicted configurations. The fine agreement between the scattered points and the colored lines indicates that the predicted results match well with the experimental law; therefore, we concluded that the mechanical model could predict the motion of the robot accurately. Then, we compared the bending curvature of the TBBs and discovered that these TBBs exhibited an approximately equal curvature that matched the bending stiffness, as shown in Figure 3C. For example, when both cables 1 and 2 are pulled by 150 mm, the bending curvature measured from experiments is $7.74 \pm 0.48 \text{ m}^{-1}$, which is only 2.17% larger than the 7.47 m^{-1} obtained from the simulation, respectively. This small difference may be ascribed to insufficient pretension in cables, and the friction between cables and/or struts is neglected in the modeling.

To elaborate on the in situ reconfigurable concept of the continuum robot, we switched the TBBs of type 1 to types 2, 3, 4, and 5, respectively, forming four other configurations with constant crosssections, marked as Cons. 2, 3, 4, and 5, as shown in Figure 4A. As the height of the types varies, the robotic length L can be programmed by regulating the types of the TBB, resulting in the configurations demonstrating diverse robotic profiles under the identical actuation criterion. The distal end trajectories of these configurations indicate that the prototype with programmable robotic length can interact with objects located within a range of distances (Figure 4B). For example, the robotic length of the Con. 5 reaches 0.60 m, 1.50 times that of the Con. 1, enabling it to be prone to interact with remote objects. Moreover, this enables the Con. 5 to develop a large enveloped area of 0.03 m^2 during grasping, which can improve the grasping stability. Then, we calculated the bending angles θ of these configurations and found that the bending angles rise linearly with the robotic lengths, following $\theta = 424.91L - 6.21$ (Figure 4C). According to the curvature formula $\rho_j = \theta_j / L_j$ ($j = 1, 2, \dots, 5$), the bending curvatures of the configurations constructed by

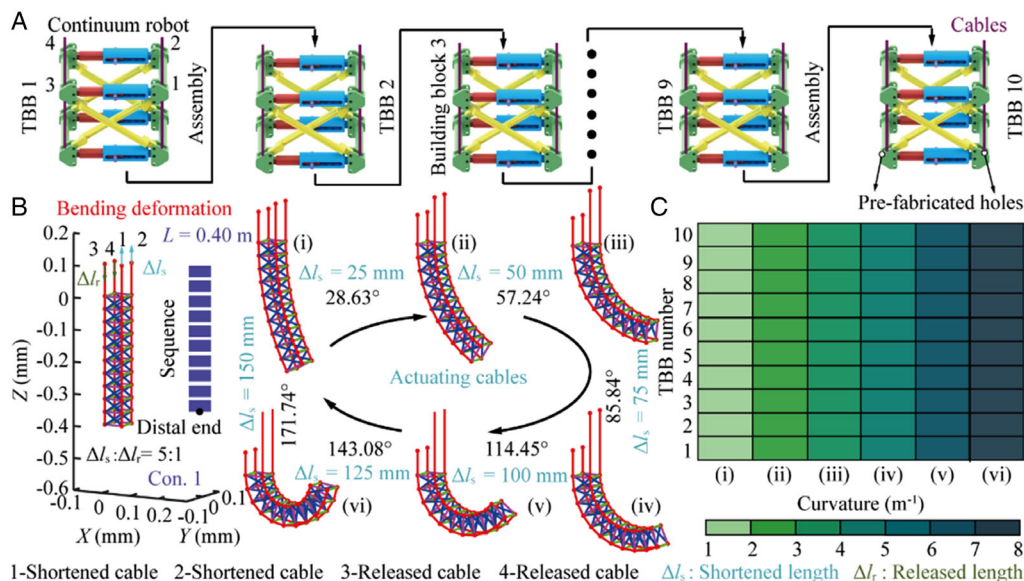


Figure 3. Bending deformation of a ten-TBB continuum robot. A) A continuum robot constructed by ten TBBs. B) Snapshots of the theoretical robotic profiles when length variations satisfy the actuation criterion. C) Changes in bending curvature of each TBB by the cable length variation.

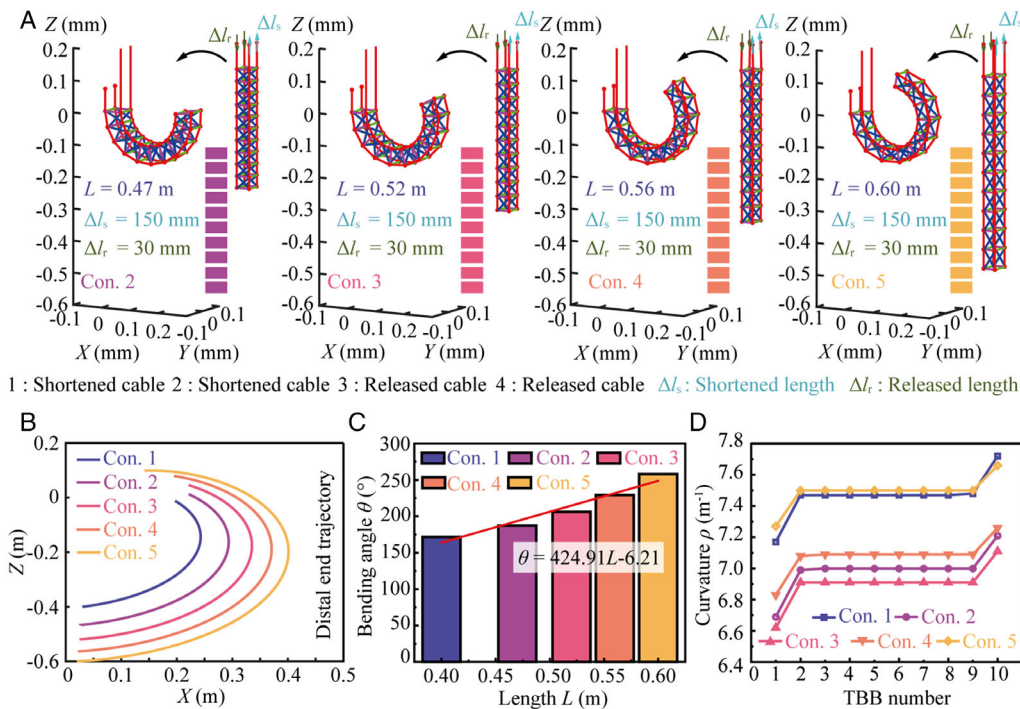


Figure 4. Continuum robot constructed by the identical homologous configuration A) Modeling morphing behaviors of the robotic configurations under the identical actuation criterion. B) Distal end trajectory of the configurations. C) Comparison of the robotic bending angle. D) Bending curvature of the blocks.

the identical type of TBBs are approximately consistent (Figure 4D). This result means that the curvature of each TBB in the configurations is approximately uniform after deformation when the robot is constructed using the identical TBB types, which may impede the application potentials of the robot to conformally interact with objects with complicated varying curvatures.

2.4. Continuum Robot Composed of Diverse Homologous TBBs

To enhance the interaction capability of the continuum robot to environments with varying curvatures, the robot with a tapered profile may be an effective scheme.^[29] Here, we programmed the type of the TBBs to develop a tapered robot. Specifically, we used the type 1 as the first TBB of the robot and then replaced the TBBs marked by the even numbers with types 1–5 in sequence, as shown in Figure 5A. Then, we introduced four transitional TBBs, which composed of stretchable struts with different lengths, to connect the aforementioned TBBs marked by the even numbers. These transitional TBBs have been marked as diverse gradient color blocks according to the type of adjacent typical homologous types. For example, the gradient color of TBB 3 is transitioned from blue to purple because it is used to connect types 1 and 2. Therefore, a new continuum robotic configuration can be reconstructed, namely, Con. 6, in which the heights of the transitional TBBs consecutively increase, as shown in Figure 5B. Then, we employed the identical actuation criterion to deform the Con. 6 and discovered that both the robotic length and

bending angle of the Con. 6 are very similar to those of the Con. 3 (Figure 5C).

In contrast to the Con. 3, each TBB of the Con. 6 exhibits diverse bending curvatures because of regulating the types of the TBBs, which is expected to enable this configuration to interact with varying-curvature objects, as shown in Figure 5D. Specifically, the transitional TBBs exhibit greater curvatures, resulting in a zig-zag curvature distribution. To analyze the causes of this distribution, we measured the bending stiffness K_B of the transitional TBBs (Figure 5E). For example, the bending stiffness of TBB 3 is $0.31 \pm 0.03\text{ N}\cdot\text{mm}/\text{deg}$, which is merely 59.62% and 72.09% that of the adjacent TBBs. As the bending stiffness of transitional TBBs is smaller than that of the adjacent TBBs, the local curvature of the Con. 6 varies and thus yields a zig-zag curvature distribution. Based on the theoretical analysis, we considered that the curvature of the robotic configuration could be regulated by combining the diverse TBBs. Hence, to further enhance the ability of the robot to interact with complicated objects, programming the distribution of the TBBs to regulate local curvature may be a feasible strategy.

2.5. Continuum Robot with Programmed Local Curvature

Taking a transitional TBB as an example, in which stretchable struts were 40 and 60 mm, we tested the strategy of regulating the local curvature of the continuum robot. First, we replaced the basal, middle, and distal locations of the Con. 1 with the two identical transitional TBBs connected through forward connection, by

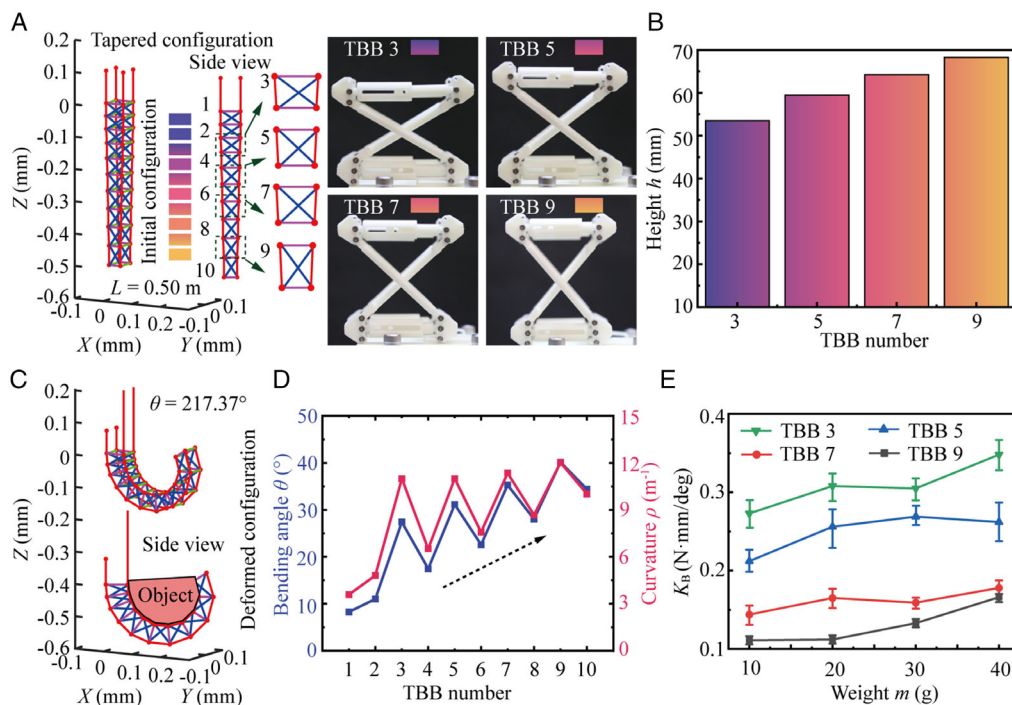


Figure 5. Bending curvature of the continuum robot with a tapered profile. A) Continuum robot with ten TBBs reconstructed into a tapered configuration. B) Height of the transitional TBBs. C) Bending profiles of the continuum robot. D) Both bending angle and curvature of the TBBs. E) Equivalent bending stiffness of the transitional TBBs.

which we formed three additional configurations, namely, Cons. 7, 8, and 9 (Figure 6A). By this, we could reach a local curvature of $17.95 \pm 0.02 \text{ m}^{-1}$, 2.55 times the curvature of TBBs that have not been tuned. This indicates that the transitional TBBs can regulate the local curvature of the robot. Although the bending angles of these configurations are approximately equal, the robot is able to conformally grasp and interact with varying-curvature objects because of the difference in the replacement position, such as the water ladle, the taro, and the fist, exhibiting greater interaction capability. Similarly, we could also connect the transitional TBBs through reverse connection and employed it to replace the basal, middle, and distal locations of the Con. 5, forming Cons. 10, 11, and 12, as shown in Figure 6B. Here, we could program the robot to adapt to the objects with different orientations. For example, the continuum robot is able to achieve conformal grasping of an apple in the orientation 1 with the Con. 10. When the apple rotated to the orientations 2 or 3, we could reconfigure the robotic configuration into the Cons. 11 or 12 to effectively grasp the apple. Therefore, we considered that reconstructing the robotic configuration in situ is a promising strategy for enhancing the interaction capability.

2.6. Application Demonstration

To evaluate the performance of the concept of in situ reconstruction, we fabricated a ten-TBB continuum robot of the Con. 1 and mounted the first TBB on a rigid robotic arm (SJ 602-A, Anno, China), as shown in Figure 7A. The continuum robot is actuated by four cables pulled by two motors (DS3135, DS-Servo, China), all of which are coordinated by a microcontroller (Uno R3,

Arduino, Italy), as shown in Figure 7B. To quantify the grasping performance of the continuum robot, we first prepared five foam balls with diverse diameters, ranging from 10 to 20 cm, to represent the objects with varying physical dimensions. Then, the continuum robot is reconstructed to the corresponding configurations to conformally interact with these foam balls (Figure 7C). As shown in Figure S5, Supporting Information, the close fitting between the robotic profile and the balls indicates that the environmental adaptability of our continuum robot can be improved by reconstructing the robotic configuration (Video S3, Supporting Information).

Then, we assumed that a potential application for our robotic system could be intelligent agriculture scenarios, owing to its high adaptability in interacting with objects in various shapes and dimensions. Specifically, harvesting robots recently have been extensively employed to reduce the working intensity of farmers. Previous farmers usually use universal agricultural machinery to collect varying agricultural products, reducing the cost of purchasing devices, because often more than one agricultural product is required to be planted in the same farm over a year.^[30] However, conventional machinery with fixed gripping apparatus cannot conformally interact with diverse agricultural products and therefore can damage them caused by excessive stress. It is estimated that the economic losses caused by mechanical damage account for 30–40% of the total agricultural output worldwide.^[31] Therefore, a reconfigurable continuum robot that can interact with the agricultural products with diverse geometrical profiles without causing a damage is an urgent requirement. Here, we demonstrated our continuum robot to grasp fruit and vegetable products (FVPs), such as apples,

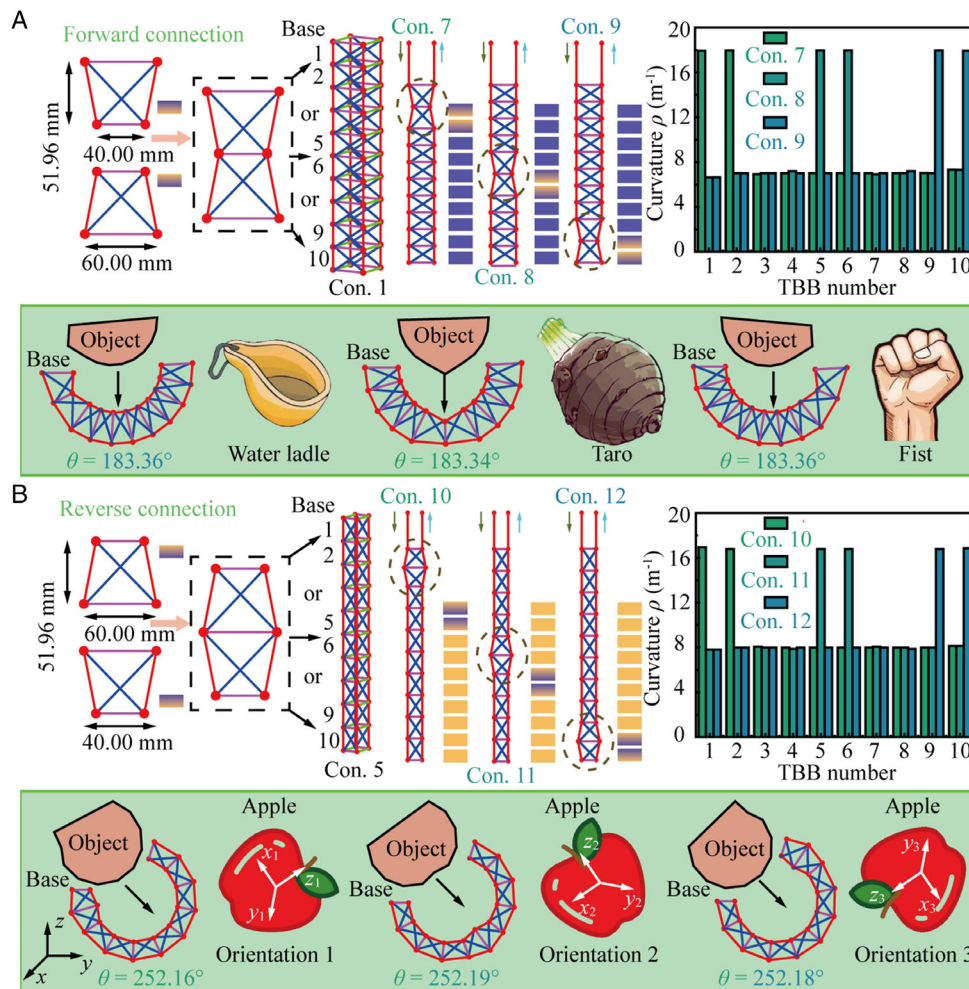


Figure 6. Programming the local curvature by introducing varying TBBs into the continuum robot. A) Regulating two adjacent TBBs at the basal, middle, or distal positions in Con. 1 with two forward connection TBBs for reconstructing the continuum robot. The reconfigurable configurations can be employed to interaction with varying objects, such as the water ladle, the taro, and the fist. B) Regulating two adjacent TBBs at the basal, middle, or distal positions in Con. 5 with two reverse connection TBBs for reconstructing the continuum robot. The reconfigurable configurations can be employed to interact with the object with varying orientations.

pineapples, mangos, pitayas, and peppers, as shown in Figure 7D (Video S4, Supporting Information). To quantify the contact force F on the surface of the FVPs during grasping, we installed a force sensor on the continuum robot, and the real-time contact force is shown in Figure 7E. Then, we evaluated the corresponding maximum contact stress σ_{\max} when the FVPs were grasped, as shown in Figure 7F. The maximum contact stress between the continuum robot and the apple is measured as 0.37 ± 0.04 MPa. Because of the conformal interaction between the continuum robot and the FVPs, the maximum contact stress in general ranges from 0.35 to 0.60 MPa, which is about an order of magnitude below the yield stress (≈ 5 MPa) of the ripe FVPs^[32]. Therefore, this continuum robot with conformal interaction capability can assist the farmers in achieving non-destructive collection/transportation of the FVPs.

Moreover, we summarized the existing cable-driven continuum robots by comparing the design scheme, actuation system layout, curvature programmability, and in situ reconfigurability,

as provided in **Table 1**, to further demonstrate the advantages of our robotic paradigm.

3. Conclusion

In this article, inspired by the structural characteristics of seahorse tails, we created an original structural template based on a programmable TBB to construct a continuum robotic paradigm. This enables us to reconstruct robotic configurations in situ to interact with varying-curvature objects, without disassembling the robot. Taking a ten-TBB continuum robot as an example, both theoretical and experimental results suggest that our proposed programmable template offers a facile and rapid reconstruction scheme of the continuum robots, which greatly improves the robotic interaction capability and overcomes time-consuming and labor-intensive limitations for programming the module type and/or arrangement sequence. Future

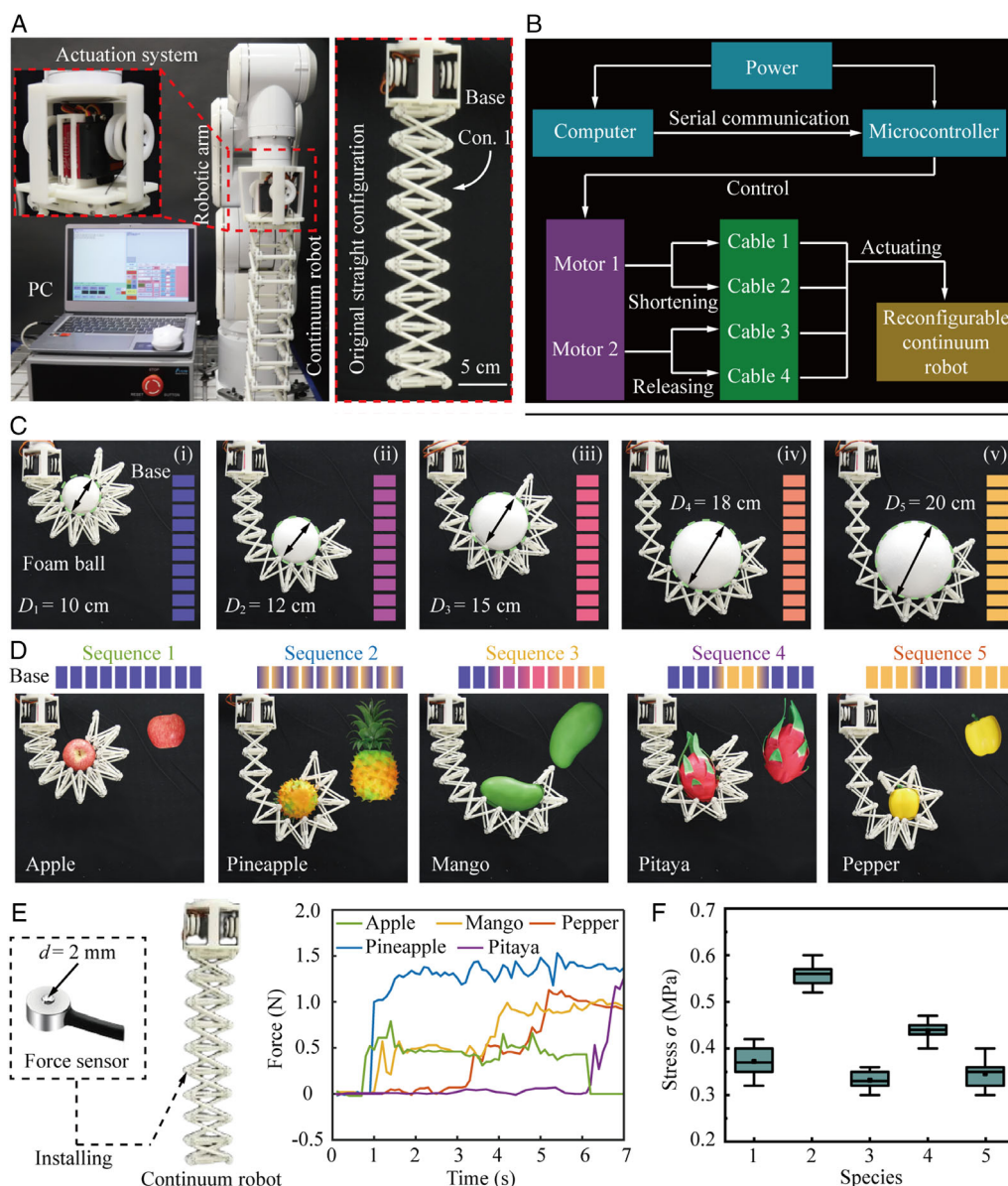


Figure 7. Application demonstration of the reconfigurable continuum robot. A) Experimental setup consisting of a 6-DOF-rigid robotic arm and our proposed continuum robot for potentially improving the mobility of the continuum robot. The original configuration of the robot with ten vertically aligned TBBs. B) Control system for the reconfigurable continuum robot. Continuum robot being able to grasp C) foam balls with diverse diameters and D) FVPs in varying geometry. E) Measurement of the contact force. (F) Maximum contact stress during grasping.

Table 1. Comparisons of the existing cable-driven continuum robots.

Authors	Modular design scheme	Remote actuation system	Programmable curvature	In situ reconfigurability
This work	✓	✓	✓	✓
Yuan ^[38]	×	✓	×	×
Santoso ^[21]	✓	×	✓	×
Wooten ^[39]	×	✓	×	×
Qin ^[40]	✓	✓	✓	×
Kim ^[41]	×	✓	✓	×

studies should develop strategies that can enhance the ability of continuum robots in interacting with varying-curvature objects in real time by adding an active modulation system, for instance, by using the advanced materials to regulate the length of the stretchable struts.^[33–35]

4. Experimental Section

Mechanical Model: To predict the configuration of the continuum robot after deformation, we employed the multi-body dynamic framework to formulate a mechanical model.^[36] Then, three assumptions were made for the components throughout the modeling to reduce the computational

complexity in the simulation. 1) The struts were considered as rigid bodies with uniform crosssections along their longitudinal axes. 2) The cables were merely subject to tension, each segment of which remained straight. 3) The friction force between the struts and cables was negligible.

Based on these assumptions, we used generalized coordinates $\mathbf{q}_i = [\mathbf{R}_i^T, \Theta_i^T]^T$ to describe the i th strut, in which \mathbf{R}_i and Θ_i denote the corresponding position vector and the orientation coordinate, respectively (Note S1, Supporting Information). To reduce the dimension of generalized coordinates, we adopted spring damping actuators to replace the function of the cables. According to the linear elastic constitutive relation, we calculated the elastic forces of the cables and formulated the internal forces in the system as $\mathbf{Q}(\mathbf{q}, t)$. By employing the constraint equations $\Phi(\mathbf{q}, t)$, these components that contain n_t transverse struts, n_l longitudinal struts, n_s stretchable struts, and n_c tension cables can be assembled. Here, the constraint force $\Phi_q^T \lambda$ was introduced into the robotic system, in which Φ_q and λ represent the Jacobian matrix and Lagrange multiples of the constraint equations, respectively. Then, we applied the actuation criterion $\mathbf{f}(\mathbf{q}, \Delta l, t)$ to actuate the robot, in which Δl represents the length variation of the cables being pulled. Therefore, the general governing equations can be written as Equation (1) (Note S1, Supporting Information)

$$\begin{cases} \Phi_q^T \lambda - \mathbf{Q} = 0 \\ \Phi(\mathbf{q}, t) = 0 \\ \mathbf{f}(\mathbf{q}, \Delta l, t) = 0 \end{cases} \quad (1)$$

Calculation of the Bending Curvature: To measure the bending curvature ρ , we first chose several points in the TBB with the coordinates of $P_i = (x_i, y_i, z_i)$.^[37] As these points were assumed to lie on the circumference of a fitting circle in XOZ plane with yet unknown radius r and the center point $P_c = (x_c, y_c, z_c)$, the circle equation can be written in the general form as Equation (2). Here, we introduced the variable $\mathbf{p} = [a, b, c]^T$ to formulate the equation in another form as Equation (3)

$$(x_i - x_c)^2 + (z_i - z_c)^2 = r^2 \quad (2)$$

$$ax_i + bz_i + c = x_i^2 + z_i^2 \quad (3)$$

When the number of the points was greater than 3, Equation (3) transforms to an equation of an overdetermined system, expressed as Equation (4). We solved this equation with help of a pseudoinverse, so the variables of the circle equation, namely, a , b , and c , can be calculated as $\mathbf{p} = \mathbf{A}^+ \mathbf{B}$, in which $\mathbf{A}^+ = (\mathbf{A}^T \mathbf{A})^{-1} \mathbf{A}^T$. Then, the curvature of the TBB can be expressed as $\rho = 1/r$

$$\underbrace{\begin{bmatrix} x_1 & z_1 & 1 \\ x_2 & z_2 & 1 \\ \dots & \dots & \dots \\ x_i & z_i & 1 \end{bmatrix}}_{\mathbf{A}} \underbrace{\begin{bmatrix} a \\ b \\ c \end{bmatrix}}_{\mathbf{p}} = \underbrace{\begin{bmatrix} x_1^2 + z_1^2 \\ x_2^2 + z_2^2 \\ \dots \\ x_i^2 + z_i^2 \end{bmatrix}}_{\mathbf{B}} \quad (4)$$

Measurement of the Equivalent Bending Stiffness: We built an experimental setup to measure the equivalent bending stiffness of the TBBs^[13]. Then, we installed a TBB on a supporting structure and applied the weight with a mass of m ($m = 10$ g, 20 g, ..., 40 g) to the TBB. Therefore, the bending angle θ was generated by the bending moment $T = mgw/2$. According to the definition of the bending stiffness $K_B = T/\theta$, we could measure the bending stiffness of the TBBs by $K_B = mgw/2\theta$.

Measurement of the Contact Stress: To evaluate the extrusion stress of the FVPs during grasping, we employed a pressure sensor (RDF-6, RuiLide, China) with a diameter of $d = 2$ mm to measure the force F between the continuum robot and the corresponding FVPs. Here, we installed the pressure sensor on the transverse strut of the TBB 5 and calculated the contact stress σ according to the formula $\sigma = \frac{4F}{\pi d^2}$.

Supporting Information

Supporting Information is available from the Wiley Online Library or from the author.

Acknowledgements

J.Z. and J.S. contributed equally to this work. The authors thank Jiangkun Wei from the School of Aeronautics and Astronautics of Sun Yat-sen University for the assistance in filming the animal behavior. This work was supported by the National Natural Science Foundation of China (grant nos. 52275298, 51905556, and U2241263) and Shenzhen Science and Technology Program (grant nos. GXWD2021B03 and 20220817165030002).

Conflict of Interest

The authors declare no conflict of interest.

Author Contributions

H.R., H.P., and J.W. conceived the concept. J.Z. and J.Y. performed the simulations. J.Z., J.S., Q.W., and J.H. carried out experiments and data processing. J.Z., H.R., and Y.Z. analyzed the data and interpreted the results. Z.W., H.P., and J.W. directed the project. All authors commented on the article.

Data Availability Statement

The data that support the findings of this study are available from the corresponding author upon reasonable request.

Keywords

conformal interaction, continuum robot, in situ reconstruction scheme, programmable curvature, tensegrity building block

Received: January 26, 2023

Revised: February 12, 2023

Published online:

- [1] G. Robinson, J. B. C. Davies, in *Proc. 1999 IEEE Int. Conf. on Robotics and Automation (Cat. No. 99CH36288C)*, IEEE, Piscataway, NJ **1999**, pp. 2849–2854.
- [2] M. F. Phelan III, M. E. Tiryaki, J. Lazovic, H. Gilbert, M. Sitti, *Adv. Sci.* **2022**, 9, 2105352.
- [3] A. Bajo, N. Simaan, *Int. J. Robot. Res.* **2016**, 35, 422.
- [4] T. George Thuruthel, E. Falotico, M. Manti, A. Pratesi, M. Cianchetti, C. Laschi, *Soft Robot.* **2017**, 4, 285.
- [5] Q. Zhao, J. Lai, K. Huang, X. Hu, H. K. Chu, *IEEE/ASME Trans. Mechatron.* **2021**, 27, 2511.
- [6] M. G. Atia, A. Mohammad, A. Gameros, D. Axinte, I. Wright, *Adv. Sci.* **2022**, 2203217.
- [7] Z. Liu, Z. Cai, H. Peng, X. Zhang, Z. Wu, *IEEE/ASME Trans. Mechatron.* **2022**.
- [8] W. Wang, S.-H. Ahn, *Soft Robot.* **2017**, 4, 379.
- [9] J. Zhang, Z. Kan, Y. Li, Z. Wu, J. Wu, H. Peng, *IEEE Robot. Automat. Lett.* **2022**, 7, 6163.
- [10] M. T. Chikhaoui, S. Lilge, S. Kleinschmidt, J. Burgner-Kahrs, *IEEE Robot. Automat. Lett.* **2019**, 4, 989.

- [11] R. Buckingham, *Industr. Robot: Int. J.* **2002**, 29, 242.
- [12] J. Yang, H. Peng, W. Zhou, J. Zhang, Z. Wu, *Mech. Mach. Theory* **2021**, 165, 104429.
- [13] X. Ke, J. Jang, Z. Chai, H. Yong, J. Zhu, H. Chen, C. Guo, H. Ding, Z. Wu, *Soft Robot.* **2022**, 9, 613.
- [14] F. Connolly, P. Polygerinos, C. J. Walsh, K. Bertoldi, *Soft Robot.* **2015**, 2, 26.
- [15] G. Z. Lum, Z. Ye, X. Dong, H. Marvi, O. Erin, W. Hu, M. Sitti, *Proc. Natl. Acad. Sci.* **2016**, 113, E6007.
- [16] J. Zhang, Y. Li, Z. Kan, Q. Yuan, H. Rajabi, Z. Wu, H. Peng, J. Wu, *Soft Robot.* **2023**.
- [17] J. L. Chien, L. T. L. Clarissa, J. Liu, J. Low, S. Foong, in *IEEE/ASME Int. Conf. on Advanced Intelligent Mechatronics*, IEEE, Piscataway, NJ **2021**, pp. 1348–1354.
- [18] Z. Jiao, C. Zhang, W. Wang, M. Pan, H. Yang, J. Zou, *Adv. Sci.* **2019**, 6, 1901371.
- [19] M. Boyvat, M. Sitti, *Adv. Sci.* **2021**, 8, 2101198.
- [20] M. A. Robertson, J. Paik, *Sci. Robot.* **2017**, 2, eaan6357.
- [21] J. Santoso, C. D. Onal, *Soft Robot.* **2021**, 8, 371.
- [22] X. Xie, D. Xiong, J. Z. Wen, *Bioinspir. Biomimet.* **2022**, 18, 016010.
- [23] S. Chen, Y. Cao, M. Sarparast, H. Yuan, L. Dong, X. Tan, C. Cao, *Adv. Mater. Technol.* **2020**, 5, 1900837.
- [24] C. Bishop, M. Russo, X. Dong, D. Axinte, *IEEE/ASME Trans. Mechatr.* **2022**, 27, 5339.
- [25] M. M. Porter, D. Adriaens, R. L. Hatton, M. A. Meyers, J. McKittrick, *Science* **2015**, 349, aaa6683.
- [26] J. Zhang, Y. Hu, Y. Li, K. Ma, Y. Wei, J. Yang, Z. Wu, H. Rajabi, H. Peng, J. Wu, *Adv. Intell. Syst.* **2022**, 2200263.
- [27] M. M. Porter, E. Novitskaya, A. B. Castro-Ceseña, M. A. Meyers, J. McKittrick, *Acta Biomater.* **2013**, 9, 6763.
- [28] J. T. Overvelde, J. C. Weaver, C. Hoberman, K. Bertoldi, *Nature* **2017**, 541, 347.
- [29] Z. Xie, A. G. Domel, N. An, C. Green, Z. Gong, T. Wang, E. M. Knubben, J. C. Weaver, K. Bertoldi, L. Wen, *Soft Robot.* **2020**, 7, 639.
- [30] W. C. Beets, *Multiple Cropping And Tropical Farming Systems*, CRC Press, Boca Raton, FL **2019**.
- [31] Y. Yamamoto, S. Fong-in, K. Kawai, *J. Food Eng.* **2021**, 307, 110649.
- [32] N. Zulkifli, N. Hashim, H. H. Harith, M. F. M. Shukery, *Trends Food Sci. Technol.* **2020**, 97, 29.
- [33] C. Tang, B. Du, S. Jiang, Q. Shao, X. Dong, X.-J. Liu, H. Zhao, *Sci. Robot.* **2022**, 7, eabm8597.
- [34] K. Bai, X. Cheng, Z. Xue, H. Song, L. Sang, F. Zhang, F. Liu, X. Luo, W. Huang, Y. Huang, Y. Zhang, *Sci. Adv.* **2020**, 6, eabb7417.
- [35] H. Zhang, J. Wu, D. Fang, Y. Zhang, *Sci. Adv.* **2021**, 7, eabf1966.
- [36] Z. Kan, H. Peng, B. Chen, W. Zhong, *Int. J. Solids Struct.* **2018**, 130, 61.
- [37] G. Runge, M. Wiese, L. Günther, A. Raatz, in *3rd Int. Conf. on Control, Automation and Robotics*, **2017**, pp. 7–14.
- [38] H. Yuan, L. Zhou, W. Xu, *Mech. Mach. Theory* **2019**, 135, 130.
- [39] M. B. Wooten, I. D. Walker, *IEEE Robot. Automat. Lett.* **2022**, 7, 10136.
- [40] G. Qin, A. Ji, Y. Cheng, W. Zhao, H. Pan, S. Shi, Y. Song, *Soft Robot.* **2022**, 9, 788.
- [41] Y. Kim, S. S. Cheng, J. P. Desai, *IEEE Trans. Robot.* **2017**, 34, 18.